SUPPLEMENTAL MATERIAL

Supplementary methods. From leaf rank to leaf age: uses and principles.

Fig. S1. Process from plant images to RER patterns.

Fig. S2. Validation of the leaf reconstruction method.

Fig. S3. Taking hyponasty into account.

Fig. S4. Effect of a severe metabolic and hydraulic constraint in combination.

Fig. S5. Heatmap of the expansion patterns for the first third of the kinetics.

Supplementary methods. From leaf rank to leaf age: uses and principles.

In order to evaluate leaf growth limitations during its development (that can last more than one month, see Aguirrezabal et al., 2006) regardless of whole plant changes like floral transition (Christophe et al., 2008), we developed an approach, fully described from Fig. S1 to Fig. S3, which consisted in translating the spatial information given by serial leaves at a given instant into a time series. The use of serial leaves of the same shoot to study changes occurring during leaf development has been recommended for long, for instance through the leaf plastochron index (Erickson and Michelini, 1957). Its relevance has been demonstrated in many species, including *Arabidopsis thaliana* grown under short day (Groot and Meicenheimer, 2000b). Ontogeny-dependent variables studied following this spatiotemporal rationale encompass leaf processes as various as expansion under water stress (Silk, 1980; Hsiao et al., 1985), morphological and anatomical changes (Isebrands and Larson, 1973; 1977; Groot and Meicenheimer, 2000a; Taylor et al., 2003), carbon balance (Silvius et al., 1978; Dickson and Larson, 1981; Kennedy and Johnson, 1981; Gagnon and Beebe, 1996; Ade-Ademilua and Botha, 2007; Reich et al., 2009), water relations (Schultz and Matthews, 1993), biomechanics (Niklas, 1991), interactions with pests (Shaik et al., 1989; Kleiner et al., 2003), or even genes expression in Arabidopsis (Efroni et al., 2008). Our method, which is based on the phyllochron age converted into time allowing a day/night representation of the data, assumes the n^{th} leaf of a stem at a given time t_1 is equivalent than the $n^{th} + 1$ older leaf at t_0, provided that $t_1 - t_0$ equals the time required for one leaf to emerge (*i.e.* the phyllochron) between leaf n and n + 1. Literature indicates that this assumption holds true for Arabidopsis rosette at least considered during a period affected neither by germination nor flowering: at 12 h photoperiod, expansion duration of successive leaves is almost constant while leaf emergence proceeds at a stable rate (Cookson et al., 2007); even at 16 h photoperiod, RER dynamics of all the 10 leaves non-preformed in the seed fitted a unique relationship (Chenu et al., 2005); above all, similar RERs and steady plastochrons were observed for more than 25 successive leaves at the 10 h photoperiod where vegetative period is extended (Groot and Meicenheimer, 2000b). We used the latter short day photoperiod and validated the assumption in our control conditions at several levels, including phyllochron, leaf area, and RER (see Fig. S2).

References cited in this section

Ade-Ademilua OE, Botha CEJ (2007) Sink to source transition in Pisum sativum leaves in relation to leaf plastochron index. Am J Plant Physiol **2**: 27-35

Aguirrezabal LAN, Bouchier-Combaud S, Radziejwoski A, Dauzat M, Cookson SJ, Granier C (2006) Plasticity to soil water deficit in Arabidopsis thaliana: dissection of leaf development into underlying growth dynamic and cellular variables reveals invisible phenotypes. Plant, Cell Environ **29**: 2216-2227

Chenu K, Franck N, Dauzat J, Barczi J-F, Rey H, Lecoeur J (2005) Integrated responses of rosette organogenesis, morphogenesis and architecture to reduced incident light in Arabidopsis thaliana results in higher efficiency of light interception. Funct Plant Biol **32**: 1123-1134

Christophe A, Letort V, Hummel I, Cournède P-H, Reffye P de, Lecoeur J (2008) A model-based analysis of the dynamics of carbon balance at the whole-plant level in Arabidopsis thaliana. Funct Plant Biol **35**: 1147-1162

Cookson SJ, Chenu K, Granier C (2007) Day length affects the dynamics of leaf expansion and cellular development in Arabidopsis thaliana partially through floral transition timing. Ann Bot **99**: 703-711

Dickson RE, Larson PR (1981) 14C fixation, metabolic labeling patterns, and translocation profiles during leaf development in Populus deltoides. Planta **152**: 461-470

Efroni I, Blum E, Goldschmidt A, Eshed Y (2008) A protracted and dynamic maturation schedule underlies Arabidopsis leaf development. Plant Cell **20**: 2293-2306

Erickson RO, Michelini FJ (1957) The plastochron index. Am J Bot **44**: 297-305

Gagnon M-J, Beebe DU (1996) Establishment of a plastochron index and analysis of the sink-to-source transition in leaves of Moricandia arvensis (L.) DC. (Brassicaceae). Int J Plant Sci **157**: 262-268

Groot EP, Meicenheimer RD (2000a) Comparison of leaf plastochron index and allometric analyses of tooth development in Arabidopsis thaliana. J Plant Growth Regul **19**: 77-89

Groot EP, Meicenheimer RD (2000b) Short-day-grown Arabidopsis thaliana satisfies the assumptions of the plastochron index as a time variable in development. Int J Plant Sci **161**: 749-756

Hsiao TC, Silk WK, Jing J (1985) Leaf growth and water deficits: biophysical effects. In NR Baker, WJ Davies, CK Ong, eds, Control of leaf growth. Cambridge University Press, New York, ppp 239-266

Isebrands JG, Larson PR (1973) Anatomical changes during leaf ontogeny in Populus deltoides. Am J Bot **60**: 199-208

Isebrands JG, Larson PR (1977) Organization and ontogeny of the vascular system in the petiole of eastern cottonwood. Am J Bot **64**: 65-77

Kennedy RA, Johnson D (1981) Changes in photosynthetic characteristics during leaf development in apple. Photosynth Res **2**: 213-223

Kleiner KW, Ellis DD, McCown BH, Raffa KF (2003) Leaf ontogeny influences leaf phenolics and the efficacy of genetically expressed Bacillus thuringiensis cry1A (a) d-endotoxin in hybrid poplar against gypsy moth. J Chem Ecol **29**: 2585-2602

Niklas KJ (1991) The elastic moduli and mechanics of Populus tremuloides (Salicaceae) petioles in bending and torsion. Am J Bot **78**: 989-996

Reich PB, Falster DS, Ellsworth DS, Wright IJ, Westoby M, Oleksyn J, Lee TD (2009) Controls on declining carbon balance with leaf age among 10 woody species in Australian woodland: do leaves have zero daily net carbon balances when they die? New Phytol **183**: 153-166

Schultz HR, Matthews MA (1993) Xylem development and hydraulic conductance in sun and shade shoots of grapevine (Vitis vinifera L.): evidence that low light uncouples water transport capacity from leaf area. Planta **190**: 393-406

Shaik M, Dickinson TA, Steadman JR (1989) Variation in rust susceptibility in beans: predicting lesion size from leaf developmental stage measured by leaf age, length, and plastochron index. Phytopathology **79**: 1035-1042

Silk WK (1980) Plastochron indices in cantaloupe grown on an irrigation line source. Bot Gaz **141**: 73-78

Silvius JE, Kremer DF, Lee DR (1978) Carbon assimilation and translocation in soybean leaves at different stages of development. Plant Physiol **62**: 54-58

Taylor G, Tricker PJ, Zhang FZ, Alston VJ, Miglietta F, Kuzminsky E (2003) Spatial and temporal effects of free-air CO2 enrichment (POPFACE) on leaf growth, cell expansion, and cell production in a closed canopy of poplar. Plant Physiol **131**: 177-185

Figure S1

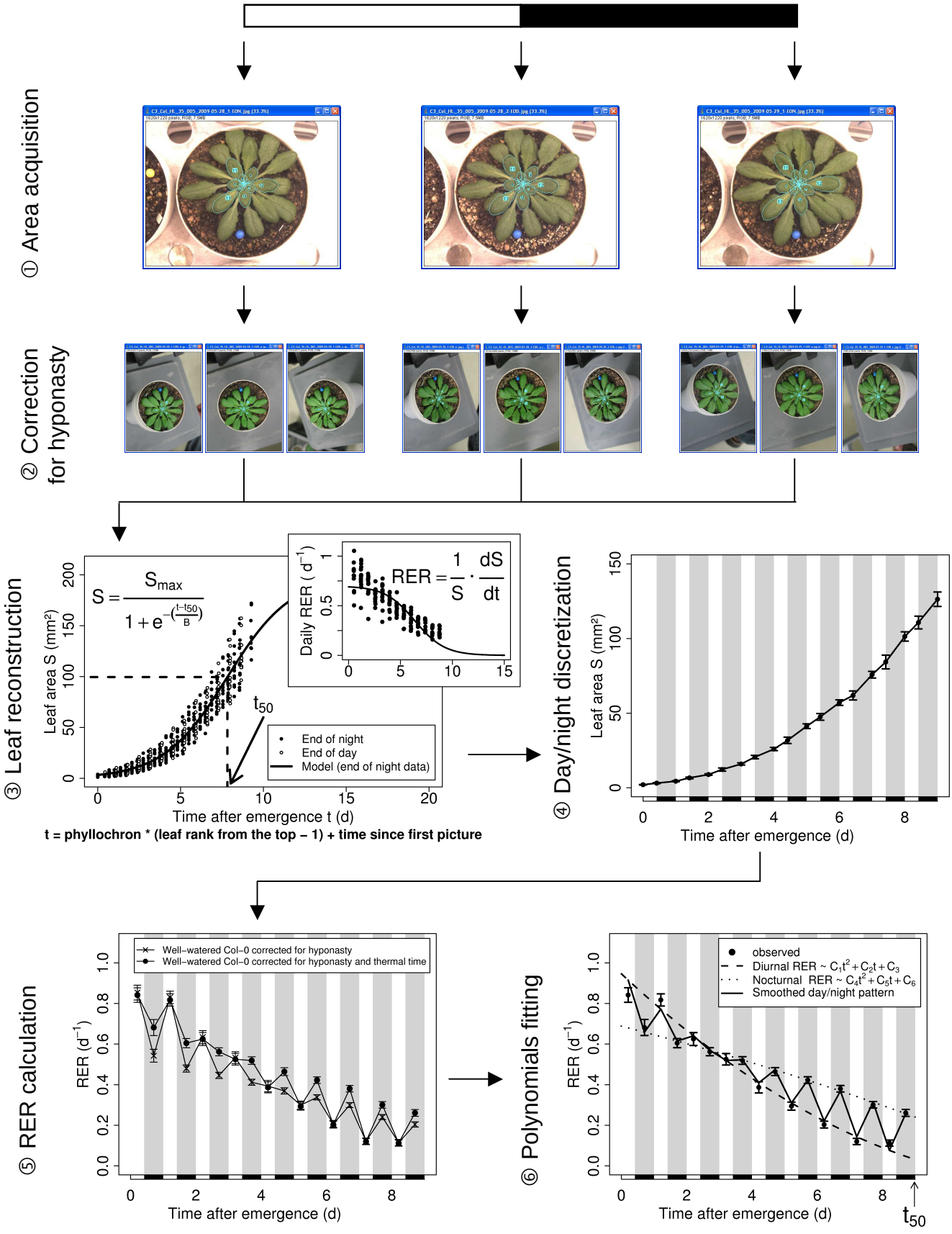
① Area acquisition
② Correction for hyponasty
③ Leaf reconstruction
④ Day/night discretization
⑤ RER calculation
⑥ Polynomials fitting
Leaf area S (mm²)
Time after emergence t (d)
Daily RER (d⁻¹)
End of night
End of day
Model (end of night data)
t50
t = phyllochron * (leaf rank from the top – 1) + time since first picture
Time after emergence (d)
RER (d⁻¹)
Well–watered Col–0 corrected for hyponasty
Well–watered Col–0 corrected for hyponasty and thermal time
observed
Diurnal RER ~ C1t²+C2t+C3
Nocturnal RER ~ C4t²+C5t+C6
Smoothed day/night pattern

Fig. S1. Process from plant images to RER patterns. When plants reached the targeted vegetative stage, three consecutive zenithal photographs were taken: the first at the beginning of a day period, the second at the end of the same day period, and the third at the end of the subsequent night. This was repeated three days later under maintained environmental regimes as a replicate, but for sake of clarity, only one session has been represented. ① **Area acquisition.** The area of serial leaves was extracted from the three pictures using a semi-automated program developed on the ImageJ software. ② **Correction for hyponasty.** An independent series of non-zenithal photographs was taken at the same three periods to measure leaf insertion angle and compute the actual leaf area. Step ② is fully described in Fig. S3 and was completed only on the wild-type Col-0 and on genotypes or environments that induced hyponasty. ③ **Leaf reconstruction.** For each picture and for each rank, leaf age after emergence was computed using the measured phyllochron. Leaf area was then plotted against its time after emergence, distinguishing end of day (open circles) from end of night (closed circles) values. the A logistical function (solid line) was fitted to the end of night dataset and the time of half expansion (t_{50}) was stored. Inset: daily relative expansion rate. RER was computed on a 24 h basis as the local slope of the natural logarithm of the area using the end of night dataset (closed circles). Analytical form of the RER (solid line) was derived from the previous logistical function and plotted using the same fitted parameters. Note that daily RER is continuously decreasing function of time. ④ **Day/night discretization.** Each area measured at the end of the day or night was assigned to the nearest reconstructed end of day or night, respectively. ⑤ **RER calculation.** RER was computed on a day/night basis using raw data (crosses) and corrected for the linear effects of temperature (thermal time, closed circles) using a threshold temperature of 3 °C and a reference temperature of 20 °C (see Methods). Values were affected to the middle of the light or dark period. ⑥ **Polynomials fitting.** A second-degree polynomial was fitted independently to the diurnal RER (dashed line) and to the nocturnal RER (dotted line). RER patterns were drawn from leaf emergence to t_{50} by joining the predicted values for the successive light and dark periods (solid line). For steps ④ to ⑥, black rectangles and gray bands indicate the night periods, and error bars are mean ± SE ($n \geq 10$).

Figure S2

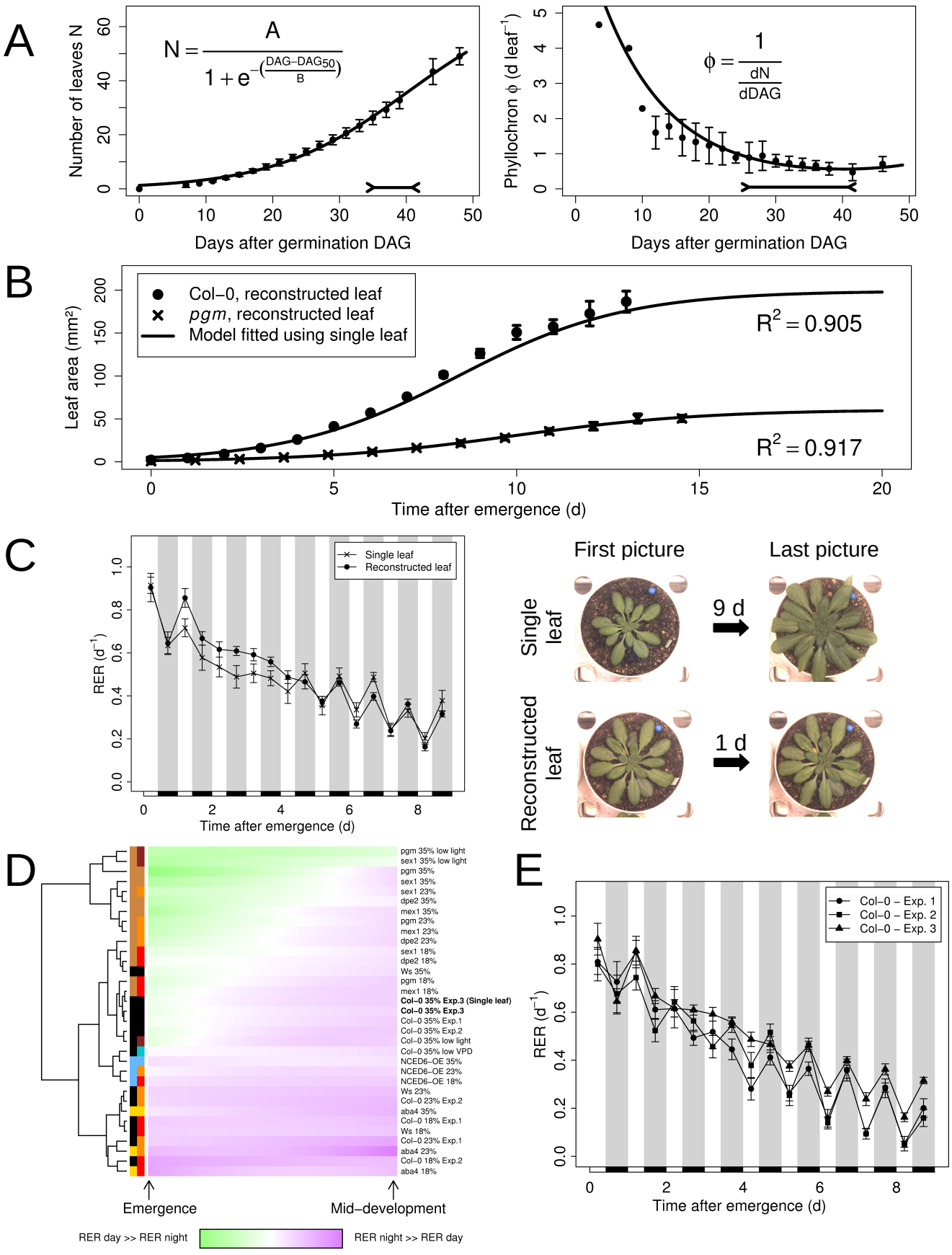
A
Number of leaves N
Days after germination DAG
Phyllochron ϕ (d leaf⁻¹)
Days after germination DAG
B
Col–0, reconstructed leaf
pgm, reconstructed leaf
Model fitted using single leaf
R² = 0.905
R² = 0.917
Leaf area (mm²)
Time after emergence (d)
C
Single leaf
Reconstructed leaf
RER (d⁻¹)
Time after emergence (d)
First picture
Last picture
Single leaf
9 d
Reconstructed leaf
1 d
D
Emergence
Mid–development
RER day >> RER night
RER night >> RER day
E
Col–0 – Exp. 1
Col–0 – Exp. 2
Col–0 – Exp. 3
RER (d⁻¹)
Time after emergence (d)

Fig. S2. Validation of the leaf reconstruction method. The relevance of the process of leaf temporal reconstruction from spatial information (Fig. S1) was verified at several levels. Error bars are mean ± SE ($n \geq 10$). **(A) Number of emerged leaves and phyllochron during rosette development.** Left panel: Emerged leaves were counted regularly until 50 days after germination (closed circles) on the well-watered Col-0. A logistical model was fitted to the data (solid line). The double-sense arrow indicates the period where the photographs were taken. Right panel: Phyllochron was computed as the inverse of leaf emergence rate, from data (closed circle) and model (solid line) of leaf number. The model was then inversed to compute the emergence date of the oldest digitalized leaf. The double-sense arrow shows the period from this oldest date until the day of measurement and underlines the phyllochron stability during this period. **(B) Area of a reconstructed leaf against a single leaf.** Leaf area was monitored either on one individual leaf during nine days (single leaf) or using serial leaves during one day (reconstructed leaf). Symbols show the area of the reconstructed leaf for Col-0 (closed circles) and *pgm* (crosses) under well-watered conditions. Solid lines show a logistical model fitted on the respective single leaf datasets. The indicated R^2 measures the quality of the model when the parameters obtained from the single leaf adjustment are applied to the reconstructed leaf dataset. **(C) Relative expansion rate of a reconstructed leaf against a single leaf.** The day/night RER in the well-watered Col-0 was compared between a reconstructed leaf and a single leaf as in (B). Black rectangles and gray bands indicate the night periods. Photographs show the whole rosette at the beginning and at the end of measurements for each method. Note that for the reconstructed leaf method, a second session was performed three days later as a replicate, leading to a four-day range between the first and the last picture, but it can be restricted to one day as depicted here. **(D) Heatmap of the expansion patterns including the single leaf dataset.** Same as Fig. 4A with addition of the single leaf data presented in (C). Note that both methods (text in bold on the right hand of the heatmap) clusterised closely together. **(E) Reproducibility of the leaf reconstruction method.** Day/night expansion patterns of a reconstructed leaf for three independent experiments performed on Col-0 under well-watered conditions. Black rectangles and gray bands indicate the night periods. Note that the three experiments clusterised closely together in the heatmap presented in (D).

Figure S3

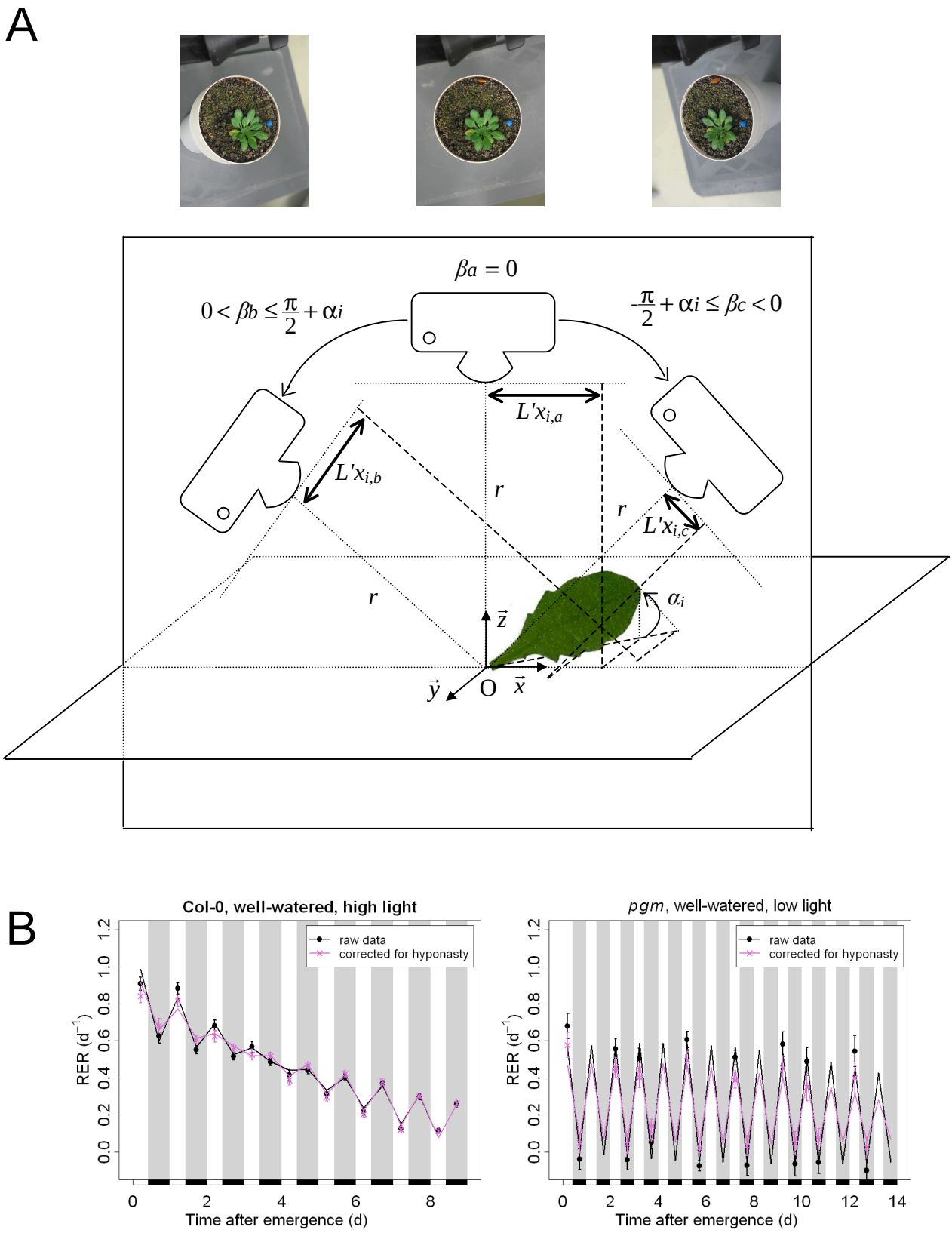
A
$\beta a = 0$
$0 < \beta b \leq \frac{\pi}{2} + \alpha i$
$-\frac{\pi}{2} + \alpha i \leq \beta c < 0$
$L'x_{i,a}$
$L'x_{i,b}$
$L'x_{i,c}$
r
r
r
α_i
$\vec{z}$
$\vec{y}$
O
$\vec{x}$
B
Col-0, well-watered, high light
pgm, well-watered, low light
raw data
corrected for hyponasty
RER (d^{-1})
Time after emergence (d)

Fig. S3. Taking hyponasty into account.

(A) Protocol to measure leaf insertion angle. Let us consider a reference frame $(\vec{x},\vec{y},\vec{z})$ of origin O related to the rosette center. Consider a digital camera whose diaphragm belongs to the circle of radius *r*, of center O and in the $(\vec{x},\vec{z})$ plane. Let β be the oriented angle between the $\vec{z}$ axis and the straight line defined by the origin and the camera diaphragm, so that for a zenithal picture, $\beta = 0$. Our camera was fixed in this way, using a rotating stand allowing to control β. Leaf length $L'x_i$ on the $\vec{x}$ component at the leaf rank *i* as measured on the photograph varies with β. Assuming that petiole and blade are aligned, the relation between the photographed leaf length $L'x_i$ and the actual leaf length Lx_i on the $\vec{x}$ component is given by:

$$\forall\ \beta \in \left[-\frac{\pi}{2}+\alpha i\ ;\ \frac{\pi}{2}+\alpha i\right]:\quad L'xi = Lxi \cdot \cos\left(\alpha i - \beta\right)$$

with α_i the insertion angle at the leaf rank *i*. One can check that the maximum of $L'x_i$ as a function of β equals Lx_i and is reached when the focal plane of the camera is parallel to the leaf plane (i.e. $\beta = \alpha_i$). Hence, using a set of three pictures { *a* ; *b* ; *c* } taken with an orientation of $\left\{\beta a = 0\ ;\ 0 < \beta b \le \frac{\pi}{2}+\alpha i\ ;\ -\frac{\pi}{2}+\alpha i \le \beta c < 0\right\}$, respectively, we were able to compute the insertion angle of each leaf rank *i* whose length on the $\vec{x}$ component was not zero, by solving numerically the following equation for α_i:

$$\frac{L'xi,b - L'xi,c}{L'xi,a} = \frac{\cos\left(\alpha i - \beta b\right) - \cos\left(\alpha i - \beta c\right)}{\cos\left(\alpha i\right)}$$

with $L'x_{i,a}$, $L'x_{i,b}$, and $L'x_{i,c}$ the length on the $\vec{x}$ component as measured on the pictures *a*, *b*, and *c*, respectively. From at least six replicates, an averaged value was computed for each leaf rank of a given genotype in a given environment, at the end of the day and at the end of the night. Then, the measured area from the zenithal pictures *S'i* of each leaf rank *i* under each condition investigated was corrected for α_i to obtain the actual area *Si* prior to the RER calculation using the simple trigonometric relationship:

$$Si = \frac{S'i}{\cos\left(\alpha i\right)}$$

(B) Examples showing the effects of leaf insertion angle on RER patterns. This protocol was applied to the well-watered Col-0 under high light as a control, and to the genotypes or treatments clearly inducing hyponasty (*pgm*, *sex1*, low light). As expected, the correction on the control had only minor effects (right panel) since Col-0 did not display a marked hyponasty. The effects were more pronounced on *pgm* under low light, a genotype × environment combination where hyponasty was enhanced, with a maximal difference of about 15 ° between night and day.

Figure S4

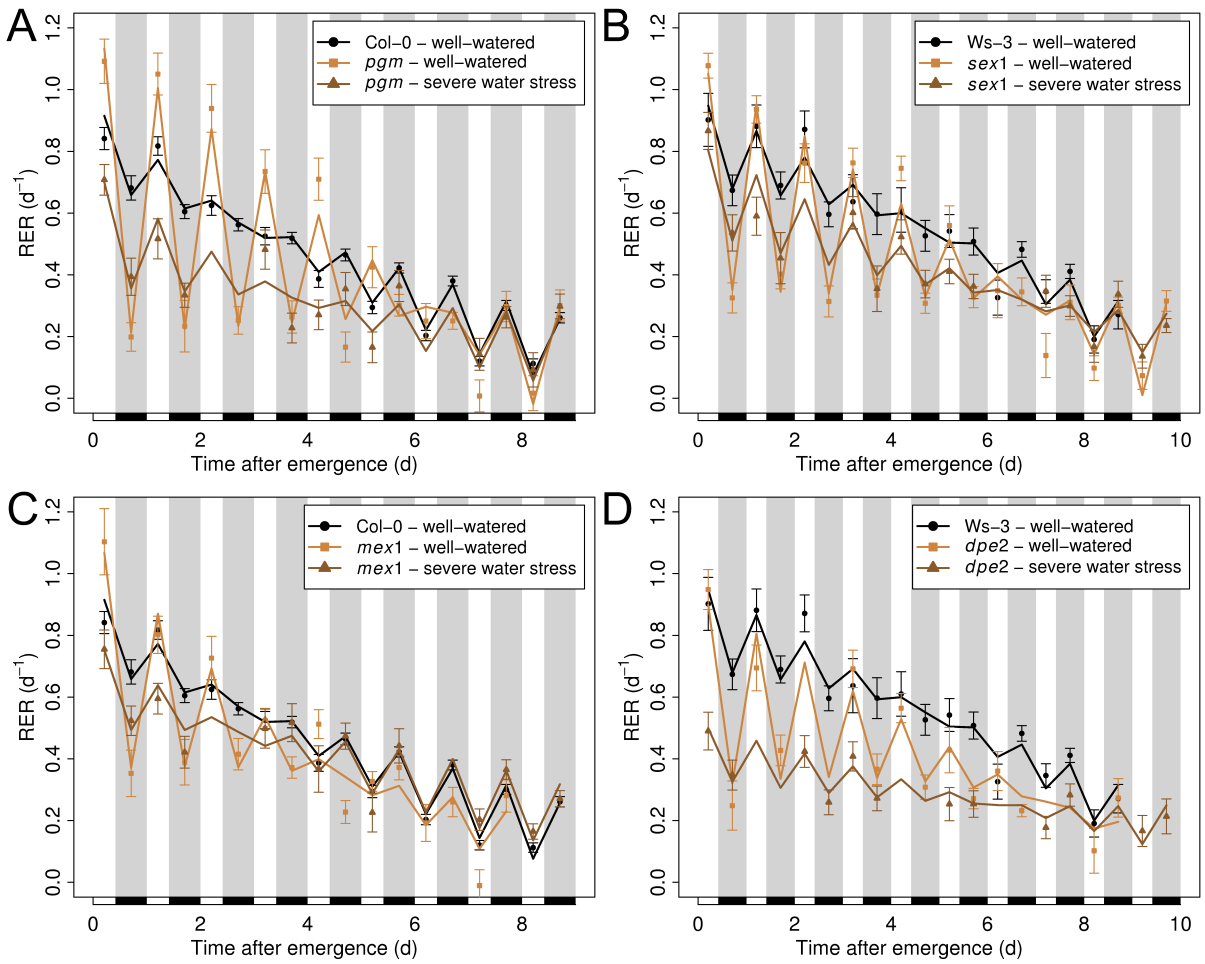

Fig. S4. Effect of a severe metabolic and hydraulic constraint in combination. The starch mutants were grown either under well-watered conditions (light tan) or under severe water stress (dark tan), and compared to their well-watered wild-type (black). Note the closeness between the starch mutants under soil water deficit and their well-watered wild-types. Black rectangles and gray bands indicate the night periods. Points: observed. Lines: smoothed. Error bars are mean ± SE (n ≥ 10). **(A) *pgm*. (B) *sex1*. (C) *mex1*. (D) *dpe2*.**

Figure S5

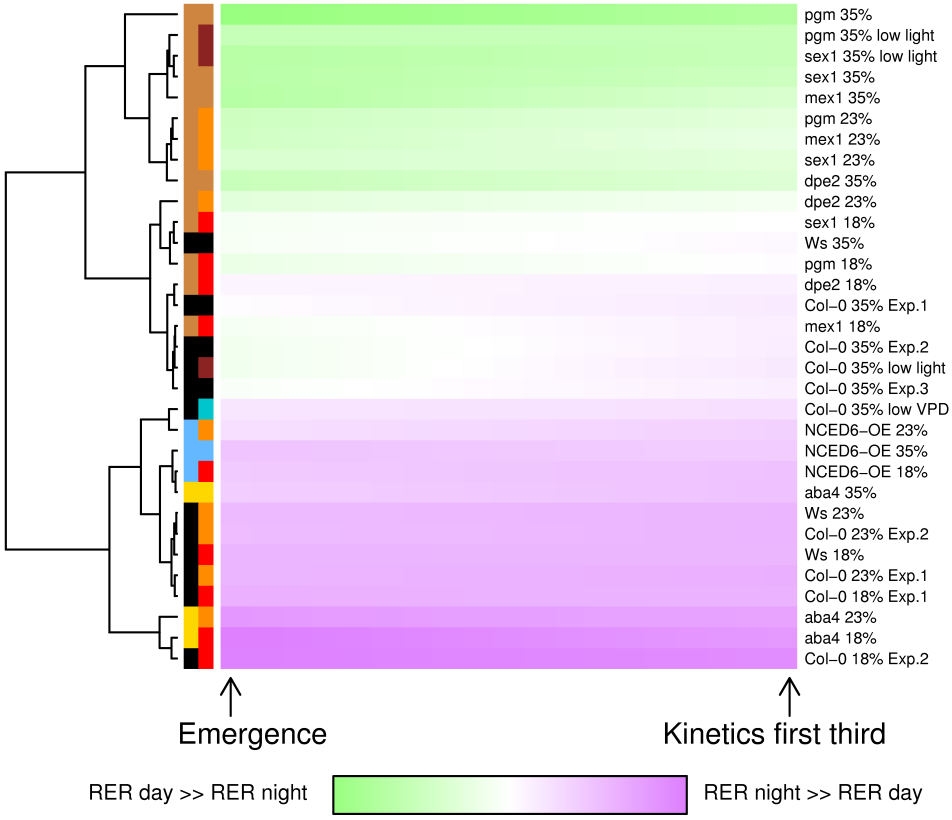

Fig. S5. Heatmap of the expansion patterns for the first third of the kinetics. Same as Fig. 4A but the analysis was restricted to the early stages. Note that in these conditions, well-watered wild-types clusterised foremost with the starch mutants instead of the wild-types under water stress.